
Invertible Autoencoder for domain adaptation

Yunfei Teng
Anna Choromanska
Mariusz Bojarski

YT1208@NYU.EDU
AC5455@NYU.EDU
MBOJARSKI@NVIDIA.COM

Abstract

The unsupervised image-to-image translation aims at finding a mapping between the source (\mathcal{A}) and target (\mathcal{B}) image domains, where in many applications aligned image pairs are not available at training. This is an ill-posed learning problem since it requires inferring the joint probability distribution from marginals. Joint learning of coupled mappings $\mathcal{F}_{AB} : \mathcal{A} \rightarrow \mathcal{B}$ and $\mathcal{F}_{BA} : \mathcal{B} \rightarrow \mathcal{A}$ is commonly used by the state-of-the-art methods, like CycleGAN (Zhu et al., 2017), to learn this translation by introducing cycle consistency requirement to the learning problem, i.e. $\mathcal{F}_{AB}(\mathcal{F}_{BA}(\mathcal{B})) \approx \mathcal{B}$ and $\mathcal{F}_{BA}(\mathcal{F}_{AB}(\mathcal{A})) \approx \mathcal{A}$. Cycle consistency enforces the preservation of the mutual information between input and translated images. However, it does not explicitly enforce \mathcal{F}_{BA} to be an inverse operation to \mathcal{F}_{AB} . We propose a new deep architecture that we call *invertible autoencoder* (*InvAuto*) to explicitly enforce this relation. This is done by forcing an encoder to be an inverted version of the decoder, where corresponding layers perform opposite mappings and share parameters. The mappings are constrained to be orthonormal. The resulting architecture leads to the reduction of the number of trainable parameters (up to 2 times). We present image translation results on benchmark data sets and demonstrate state-of-the-art performance of our approach. Finally, we test the proposed domain adaptation method on the task of road video conversion. We demonstrate that the videos converted with InvAuto have high quality and show that the NVIDIA neural-network-based end-to-end learning system for autonomous driving, known as PilotNet, trained on real road videos performs well when tested on the converted ones.

1. Introduction

Inter-domain translation problem of converting an instance, e.g.: image or video, from one domain to another is applicable to a wide variety of learning tasks, including object detection and recognition, image categorization, sentiment analysis, action recognition, speech recognition, and more. High-quality domain translators ensure that an arbitrary learning model trained on the samples from the source domain, can perform well when tested on the translated samples¹. The translation problem can be posed in the supervised learning framework, e.g.: (Isola et al., 2017; Wang et al., 2017), where the learner has access to corresponding pairs of instances from both domains, or unsupervised learning framework, e.g.: (Zhu et al., 2017; Liu et al., 2017), where no such paired instances are available. This paper focuses on the latter case, which is more difficult but at the same time more realistic as acquiring the data set of paired images is often impossible in practice.

The unsupervised domain adaptation is typically solved using generative adversarial networks (GAN) framework (Goodfellow et al., 2014), where the generator performs domain translation and is trained to learn the mapping from the source to the target domain and the discriminator is trained to discriminate between original images from the target domain and those provided by the generator. In this setting, the generator usually has the structure of the autoencoder. The two most common state-of-the-art domain adaptation approaches, CycleGAN (Zhu et al., 2017) and UNIT (Liu et al., 2017), are built on this basic approach. CycleGAN addresses the problem of adaptation from domain \mathcal{A} to domain \mathcal{B} by training two translation networks, where one realizes the mapping \mathcal{F}_{AB} and the other realizes \mathcal{F}_{BA} . The cycle consistency loss ensures the correlation between input image and the corresponding translation. In particular, to achieve cycle consistency, CycleGAN trains two autoencoders, where each minimizes its own adversarial loss and they both jointly minimize

$$\|\mathcal{F}_{AB}(\mathcal{F}_{BA}(\mathcal{B})) - \mathcal{B}\|_2^2 \text{ and } \|\mathcal{F}_{BA}(\mathcal{F}_{AB}(\mathcal{A})) - \mathcal{A}\|_2^2. \quad (1)$$

¹Similarly, an arbitrary learning model trained on the translated samples should perform well on the samples from the target domain. Training in this framework is however much more computationally expensive.

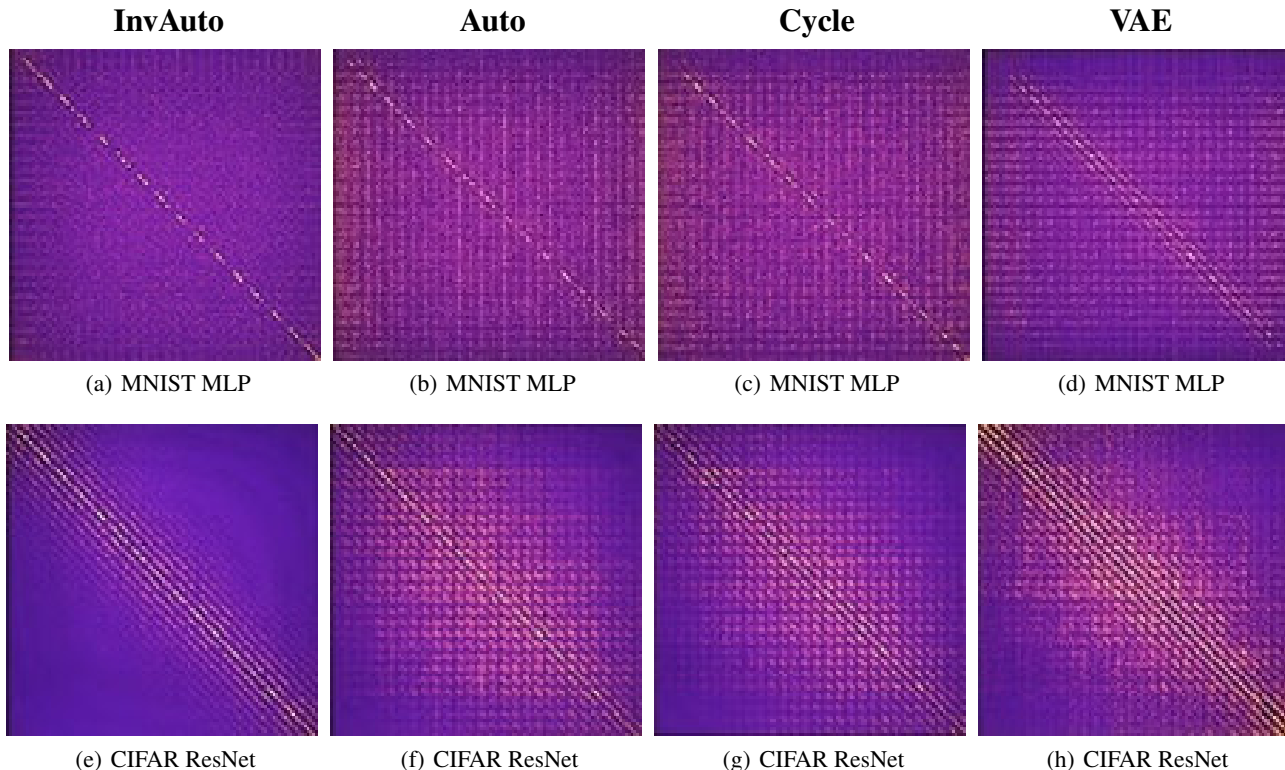


Figure 1. Heatmap of the values of matrix DE for InvAuto (a and e), Auto (b and f), Cycle (c and g), and VAE (d and h) on MLP and ResNet architectures and MNIST and CIFAR data sets. Matrices E and D are constructed by multiplying the weight matrices of consecutive layers of encoder and decoder, respectively. In case of InvAuto, DE is the closest to the identity matrix.

Cycle consistency loss is also incorporated into the recent implementations of UNIT. It is implicitly assumed that the model will learn the mappings \mathcal{F}_{AB} and \mathcal{F}_{BA} in such a way that $\mathcal{F}_{AB} = \mathcal{F}_{BA}^{-1}$, however it is not explicitly imposed. Consider a simple example. Assume the first autoencoder is a 2-layer linear multi-layer perceptron (MLP) where the weight matrix of the first layer (encoder) is denoted as E_1 and the weight matrix of the second layer (decoder) is denoted as D_1 . Thus, for an input $x_A \in \mathcal{A}$ it outputs $y_B(x_A) = D_1 E_1 x_A$. The second autoencoder then is a 2-layer MLP with encoder weight matrix E_2 and decoder weight matrix D_2 that for an input data point x_B should produce output $y_A(x_B) = D_2 E_2 x_B$. To satisfy cycle consistency requirement, the following should hold: $y_A(y_B(x_A)) = x_A$ and $y_B(y_A(x_B)) = x_B$. These two conditions are equivalent to $D_2 E_2 D_1 E_1 = I$ and $D_1 E_1 D_2 E_2 = I$. This holds for example when $D_1 = E_2^{-1}$ and $D_2 = E_1^{-1}$.

In contrast to this approach, we implicitly require $\mathcal{F}_{AB} = \mathcal{F}_{BA}^{-1}$. Thus, in the context of the given simple example, we correlate encoders and decoders to satisfy inversion conditions $D_1 = E_2^{-1}$ and $D_2 = E_1^{-1}$. We avoid performing prohibitive inversions of large matrices and instead guarantee these conditions to hold through two steps: (i) introducing shared parametrization of encoder E_2 and decoder D_1 such that $D_1 = E_2^{-1}$ (E_1 and D_2 is treated simi-

larly) and (ii) appropriate training to achieve orthonormality $E_2^\top = E_2^{-1}$ and $E_1^\top = E_1^{-1}$, i.e. we train autoencoder (E_2, D_1) to satisfy $D_1 E_2 x_B = x_B$ for arbitrary input x_B and autoencoder (E_1, D_2) to satisfy $D_2 E_1 x_A = x_A$ for arbitrary input x_A . Since the encoder and decoder are coupled as given in (i), such training leads to satisfying inversion conditions. Practical networks contain linear and non-linear transformations. We therefore propose specific architectures, which are invertible.

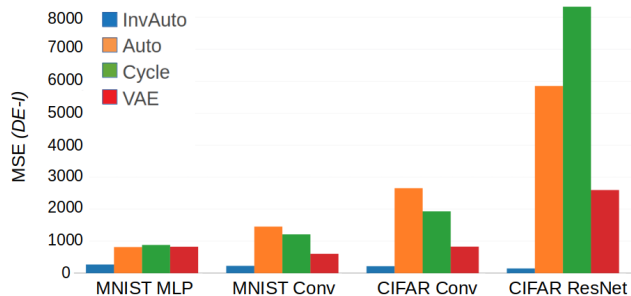


Figure 2. Comparison of the mean squared error (MSE) $MSE(DE - I)$ for InvAuto, Auto, Cycle, and VAE on MLP, convolutional, and ResNet architectures and MNIST and CIFAR data sets. Matrices E and D are constructed by multiplying the weight matrices of consecutive layers of encoder and decoder, respectively.

Figure 1 (see also its extended version, Figure 17, in the Supplement) and 2 illustrate the basic idea behind InvAuto. The plots were obtained by training a single autoencoder (E, D) to reconstruct its input. InvAuto has shared weights satisfying $D = E^\top$ and inverted non-linearities and clearly obtains matrix DE that is the closest to identity compared to other methods, i.e. vanilla autoencoder (Auto), autoencoder with cycle consistency (Cycle), and variational autoencoder (VAE) (Kingma & Welling, 2014). Note also that at the same time InvAuto requires half of the number of trainable parameters.

This paper is organized as follows: Section 2 reviews the literature, Section 3 explains InvAuto in details, Section 4 explains how to apply InvAuto to domain adaptation, Section 5 demonstrates experimental verification of the proposed approach, and Section 6 provides conclusions.

2. Related Work

Unsupervised image-to-image translation models were developed to tackle domain adaptation problem with unpaired data sets. A plethora of existing approaches utilize autoencoders trained in the GAN framework, where autoencoder serves as a generator, for this learning problem. This includes approaches based on conditional GAN (Dong et al., 2017; Wang et al., 2017) and methods introducing additional components to the loss function forcing partial cycle consistency (Taigman et al., 2016). Another approach (Liu & Tuzel, 2016) introduces two coupled GANs, where each generator is an autoencoder and the coupling is obtained by sharing a subset of weights between autoencoders as well as between discriminators. This technique was later on extended to utilize variational autoencoders as generators (Liu et al., 2017). The resulting approach is commonly known as UNIT. CycleGAN presents yet another way of addressing the image-to-image translation by specific training scheme that preserves the mutual information between input and translated images (Vincent et al., 2008). Both UNIT and CycleGAN constitute the most popular choices for performing image-to-image translation.

There also exist other learning tasks that can be viewed as instances of image-to-image translation problem. Among them, notable approaches focus on style transfer (Gatys et al., 2016b; Johnson et al., 2016; Ulyanov et al., 2016; Gatys et al., 2016a). They aim at preserving the content of the input image while altering its style to mimic the style of the images from the target domain. This goal is achieved by introducing content and style loss functions that are jointly optimized. Finally, inverse problems, such as super-resolution, also fall into the category of image-to-image translation problems (McCann et al., 2017).

3. Invertible autoencoder

Here we explain the details of the architecture of InvAuto. The architecture needs to be symmetric to allow invertibility, e.g.: the layers should be arranged as $(\underbrace{T_1, T_2, \dots, T_M}_{\text{encoder } E}, \underbrace{T_M^{-1}, T_{M-1}^{-1}, \dots, T_1^{-1}}_{\text{decoder } D})$, where

T_1, T_2, \dots, T_M denote subsequent transformations of the signal that is being propagated through the network (M is the total number of those) and $T_1^{-1}, T_2^{-1}, \dots, T_M^{-1}$ denote their inversions. Thus, the architecture is inverted layer by layer, where any layer of the encoder has its mirror inverted counterpart in the decoder. The autoencoder is trained to reconstruct its input. Below we explain how to invert different types of layers of the deep model.

3.1. Fully-connected layer

Consider transformation T^E of an input signal performed by an arbitrary fully-connected layer of an encoder E parametrized with weight matrix W . Let x denote layer’s input and y denote its output. Thus

$$T^E : y = Wx. \quad (2)$$

An inverse operation is then defined as

$$(T^E)^{-1} : x = W^{-1}y, \quad (3)$$

We parametrize the counterpart layer of the decoder with a transpose of W , thus the considered encoder and decoder layers will share parametrization. Therefore, we enforce the counterpart decoder’s layer to perform transformation:

$$T^D : x = W^\top y. \quad (4)$$

By training the autoencoder to reconstruct its input on its output we will enforce orthonormality $W^{-1} = W^\top$ and thus equivalence of transformations $(T^E)^{-1}$ and T^D , i.e. $(T^E)^{-1} \equiv T^D$.

3.2. Convolutional layer

Consider transformation T^E of an input image performed by an arbitrary convolutional layer of an encoder E . Let x denote layer’s vectorized input image and y denote corresponding output. 2D convolution can be implemented using matrix multiplication involving a Toeplitz matrix (Vasudevan et al., 2017). Toeplitz matrix is obtained from the set of kernels of the 2D convolutional filters. Thus transformation T^E and its inverse $(T^E)^{-1}$ can be explained with the same equations as the ones used before, Equations 2 and 8, however now W is a Toeplitz matrix. We will again parametrize the counterpart layer of the decoder with a transpose of a Toeplitz matrix W . The transpose of the Toeplitz matrix is in practice obtained by copying weights from the considered convolutional layer to the counterpart decoder’s layer that is implemented as a transposed convolutional layer (also known as a deconvolutional layer).

Therefore, as before, we enforce the counterpart decoder’s layer to perform transformation $T^D : x = W^\top y$ and by appropriate training ensure $(T^E)^{-1} \equiv T^D$.

3.3. Activation function

Invertible activation function should be a bijection. In this paper we consider a modified LeakyReLU activation function σ and use only this non-linearity in the model. Consider transformation T^E of an input signal performed by this non-linearity applied in the encoder E . This non-linearity is defined as

$$T^E : y = \sigma(x) = \begin{cases} \frac{1}{\alpha}x, & \text{if } x \geq 0 \\ \alpha x, & \text{otherwise.} \end{cases} \quad (5)$$

An inverse operation is then defined as

$$(T^E)^{-1} : x = \sigma^{-1}(y) = \begin{cases} \alpha y, & \text{if } y \geq 0 \\ \frac{1}{\alpha}y, & \text{otherwise.} \end{cases} \quad (6)$$

The corresponding non-linearity in the decoder will therefore realize the operation of an inverted modified LeakyReLU given in Equation 6. In the experiments we set $\alpha = 2$.

3.4. Residual block

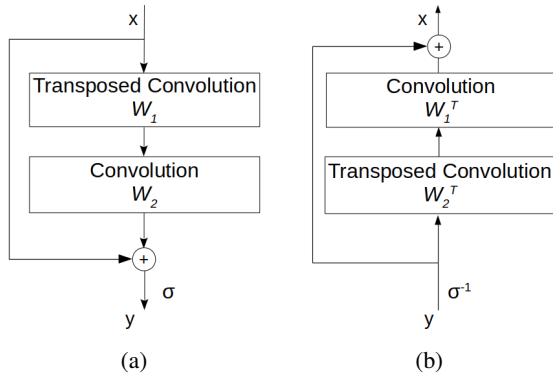


Figure 3. (a) Residual block. (b) Inverted residual block.

Consider transformation T^E of an input signal performed by a residual block (He et al., 2016) of an encoder E . We modify the residual block to remove the internal non-linearity as given in Figure 3a. The residual block is parametrized with weight matrices W_1 and W_2 . Those are Toeplitz matrices corresponding to the convolutional and transposed convolutional layers of the residual block. Let x denote block’s vectorized input and y denote its corresponding output. Thus transformation T^E is defined as

$$T^E : y = \sigma((W_2 \cdot W_1 + I) \cdot x) \quad (7)$$

An inverse operation is then defined as

$$(T^E)^{-1} : x = (W_2 \cdot W_1 + I)^{-1} \sigma^{-1}(y). \quad (8)$$

We will parametrize the counterpart residual block of the decoder with a transpose of matrix $W_2 \cdot W_1 + I$ as given in Figure 3b. Therefore we enforce the counterpart decoder’s residual block to perform transformation:

$$T^D : x = (W_1^\top W_2^\top + I)y. \quad (9)$$

Similarly as before, at training will enforce orthonormality $(W_2 \cdot W_1 + I)^{-1} = (W_2 \cdot W_1 + I)^\top$ and thus $(T^E)^{-1} \equiv T^D$.

3.5. Bias

We consider bias as a separate layer in the network. Then, handling biases is straightforward. In particular, the layer in the encoder that perform bias addition has its counterpart layer in the decoder, where the same bias is subtracted.

3.6. Experimental validation of orthonormality

In this section, we validate the concept of InvAuto. The goal of this section is to show that proposed shared parametrization and training enforce orthonormality and that at the same time the orthonormality property is not organically achieved by standard architectures. We compare InvAuto with previously mentioned vanilla autoencoder, autoencoder with cycle consistency, and variational autoencoder. We experimented with various data sets (MNIST and CIFAR-10) and architectures (MLP, convolutional (Conv), and ResNet). All the networks were designed to have 2 down-sampling layers and 2 up-sampling layers. Encoder’s matrix E and decoder’s matrix D are constructed by multiplying the weight matrices of consecutive layers of encoder and decoder, respectively.

Data set and model	InvAuto	Auto	Cycle	VAE
MNIST MLP	0.001 ± 0.118	0.008 ± 0.210	0.007 ± 0.207	0.001 ± 0.219
MNIST Conv	0.001 ± 0.148	0.001 ± 0.179	0.001 ± 0.176	-0.001 ± 0.190
CIFAR Conv	0.001 ± 0.145	0.002 ± 0.176	0.004 ± 0.195	0.003 ± 0.268
CIFAR ResNet	0.000 ± 0.134	0.000 ± 0.203	0.000 ± 0.232	0.001 ± 0.298

Table 1. Mean and standard deviation of cosine similarity of rows of E . InvAuto achieves cosine similarity that is the closest to 0.

We test orthonormality by reporting the histograms of the cosine similarity of each pair of rows of matrix E for all methods (Figure 4) along with their mean and standard deviation (Table 1) as we expect the cosine similarity to be close to 0 for InvAuto. We then show the ℓ_2 -norm of the rows of E as we expect the rows of InvAuto to have close-to-unit norm (Table 2). InvAuto enforces the encoder, and consequently the decoder, to be orthonormal. Other methods do not explicitly demand that and thus the orthonormality of their encoders is weaker. This observation is further

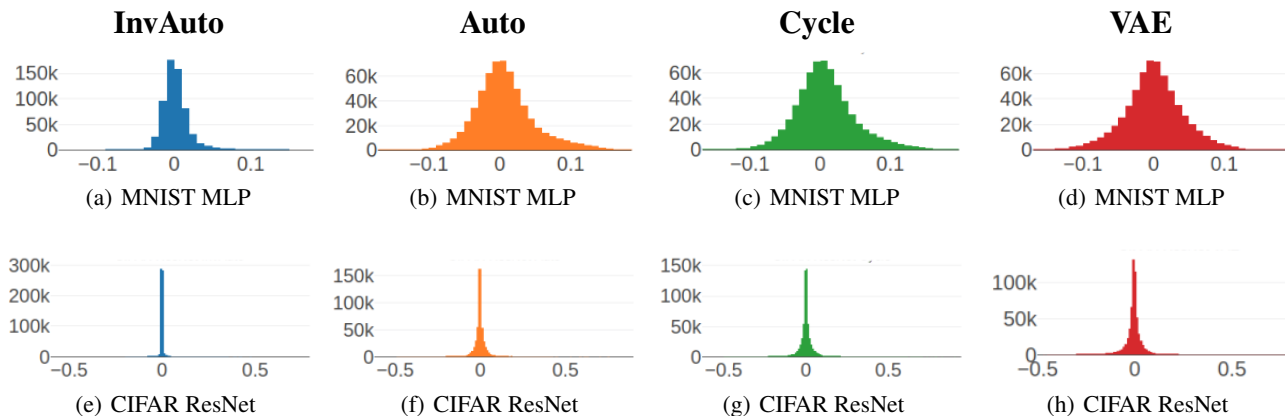


Figure 4. The histograms of cosine similarity of the rows of E for InvAuto (a and e), Auto (b and f), Cycle (c and g), and VAE (d and p) on MLP and ResNet architectures and MNIST and CIFAR data sets.

Data set and model	InvAuto	Auto	Cycle	VAE
MNIST MLP	0.976 ± 0.190	1.326 ± 0.095	1.268 ± 0.095	1.832 ± 0.501
MNIST Conv	0.905 ± 0.321	1.699 ± 0.732	1.780 ± 0.779	1.971 ± 0.794
CIFAR Conv	0.908 ± 0.219	3.027 ± 0.816	2.463 ± 0.688	1.176 ± 0.356
CIFAR ResNet	0.868 ± 0.078	2.890 ± 0.895	2.650 ± 0.937	1.728 ± 0.311

Table 2. Mean and standard deviation of the ℓ_2 -norm of the rows of E . InvAuto achieves the ℓ_2 -norm of the rows that is the closest to the unit norm.

confirmed by Figures 1 and 2 shown before in the Introduction. In the Supplement (Section A), we provide three more figures that complement Figure 2 (recall that the latter reports the MSE of $DE - I$). They show the MSE of the diagonal (Figure 14) and off-diagonal of $DE - I$ (Figure 15) as well as the ratio of the MSE of the off-diagonal and diagonal of DE (Figure 16) for various methods. The reconstruction loss obtained for all methods is also shown in Section A in the Supplement (Table 5).

Next we describe how InvAuto is applied to the problem of domain adaptation.

4. Invertible autoencoder for domain adaptation

For the purpose of performing domain adaptation we construct the dedicated architecture that is similar to CycleGAN, but we use InvAuto at the feature level of the generators. This InvAuto contains encoder E and decoder D that themselves have the form of autoencoders. Each of these internal autoencoders is used to do the conversion between the features corresponding to two different domains. And thus, the encoder E performs the conversion from the features corresponding to domain \mathcal{A} into the features corre-

sponding to domain \mathcal{B} . The decoder D , on the other hand, performs the conversion from the features corresponding to domain \mathcal{B} into the features corresponding to domain \mathcal{A} . Since E and D form InvAuto, E realizes an inversion of D (and vice versa) and shares parameters with D . This introduces strong correlations between two generators and reduces the number of trainable parameters, which distinguishes our approach from CycleGAN. The proposed architecture is illustrated in Figure 5. The details of the architecture and training are provided in Section C in the Supplement.

Next we describe the cost function that we use to train our deep model. The first component of the cost function is the adversarial loss (Goodfellow et al., 2014), i.e.

$$\begin{aligned}
 L_{\text{adv}}(\text{Gen}_{\mathcal{A}}, \text{Dis}_{\mathcal{A}}) &= \mathbb{E}_{x_{\mathcal{A}} \sim p_d(\mathcal{A})} [\log \text{Dis}_{\mathcal{A}}(x_{\mathcal{A}})] + \\
 &\quad \mathbb{E}_{x_{\mathcal{B}} \sim p_d(\mathcal{B})} [\log(1 - \text{Dis}_{\mathcal{A}}(\text{Gen}_{\mathcal{A}}(x_{\mathcal{B}})))] \\
 L_{\text{adv}}(\text{Gen}_{\mathcal{B}}, \text{Dis}_{\mathcal{B}}) &= \mathbb{E}_{x_{\mathcal{B}} \sim p_d(\mathcal{B})} [\log \text{Dis}_{\mathcal{B}}(x_{\mathcal{B}})] + \\
 &\quad \mathbb{E}_{x_{\mathcal{A}} \sim p_d(\mathcal{A})} [\log(1 - \text{Dis}_{\mathcal{B}}(\text{Gen}_{\mathcal{B}}(x_{\mathcal{A}})))] ,
 \end{aligned} \tag{10}$$

where $p_d(\mathcal{A})$ and $p_d(\mathcal{B})$ denote the distribution of data from \mathcal{A} and \mathcal{B} , respectively.

The second component of the loss function is the cycle consistency loss defined as

$$\begin{aligned}
 L_{\text{cc}}(\text{Gen}_{\mathcal{A}}, \text{Gen}_{\mathcal{B}}) &= \mathbb{E}_{x_{\mathcal{A}} \sim p_d(\mathcal{A})} [\|x_{\mathcal{A}} - \text{Gen}_{\mathcal{A}}(\text{Gen}_{\mathcal{B}}(x_{\mathcal{A}}))\|_1] \\
 &\quad + \mathbb{E}_{x_{\mathcal{B}} \sim p_d(\mathcal{B})} [\|x_{\mathcal{B}} - \text{Gen}_{\mathcal{B}}(\text{Gen}_{\mathcal{A}}(x_{\mathcal{B}}))\|_1] .
 \end{aligned} \tag{11}$$

The objective function that we minimize therefore becomes

$$\begin{aligned}
 L(\text{Gen}_{\mathcal{A}}, \text{Gen}_{\mathcal{B}}, \text{Dis}_{\mathcal{A}}, \text{Dis}_{\mathcal{B}}) &= \lambda L_{\text{cc}}(\text{Gen}_{\mathcal{A}}, \text{Gen}_{\mathcal{B}}) \\
 &\quad + L_{\text{adv}}(\text{Gen}_{\mathcal{A}}, \text{Dis}_{\mathcal{A}}) \\
 &\quad + L_{\text{adv}}(\text{Gen}_{\mathcal{B}}, \text{Dis}_{\mathcal{B}}),
 \end{aligned} \tag{12}$$

where λ controls the balance between the adversarial loss and cycle consistency loss. The cycle consistency loss enforces the orthonormality property of InvAuto.

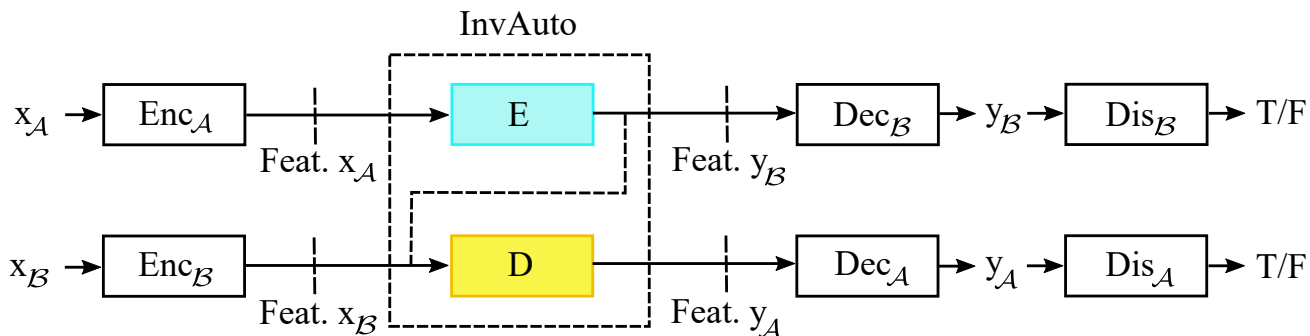


Figure 5. The architecture of the domain translator with InvAuto (E, D). $x_A \in \mathcal{A}$ and $x_B \in \mathcal{B}$ are the inputs of the translator. y_B is a converted image x_A into the \mathcal{B} domain and y_A is a converted image x_B into the \mathcal{A} domain. Invertible autoencoder (E, D) is built of encoder E and decoder D , where each of those itself is an autoencoder. $\text{Enc}_A, \text{Enc}_B$ are feature extractors, and $\text{Dec}_A, \text{Dec}_B$ are the final layers of the generators Gen_B , i.e. $(\text{Enc}_A, E, \text{Dec}_B)$, and Gen_A , i.e. $(\text{Enc}_B, D, \text{Dec}_A)$, respectively. Discriminators Dis_A and Dis_B discriminate whether their input comes from the generator (True) or original data set (False).

5. Experiments

We next demonstrate the experiments on domain adaptation problems. We compare our model against UNIT(Liu et al., 2017) and CycleGAN(Zhu et al., 2017). We used publicly available implementations of both methods available from <https://github.com/mingyuliutw/UNIT/> and <https://github.com/junyanz/pytorch-CycleGAN-and-pix2pix/>. The details of our architecture and the training process are summarized in Section C in the Supplement.

5.1. Experiments with benchmark data sets

We considered the following domain adaptation tasks:

- (i) Day-to-night and night-to-day image conversion: we used unpaired road pictures recorded during the day and at night obtained from KAIST data set (Hwang et al., 2015).
- (ii) Day-to-thermal and thermal-to-day image conversion: we used road pictures recorded during the day with a regular camera and a thermal camera obtained from KAIST data set(Hwang et al., 2015).
- (iii) Maps-to-satellite and satellite-to-maps: we used satellite images and maps obtained from Google Maps (Isola et al., 2017).

The data sets for the last two tasks, i.e. (ii) and (iii), are originally paired, however we randomly permuted them and train the model in an unsupervised fashion. The training and testing images were furthermore resized to 128×128 resolution.

The visual results of image conversion are presented in Figures 6-11 (Section B in the Supplement contains the same figures in higher resolution). We see that InvAuto visually performs comparably to other state-of-the-art methods.

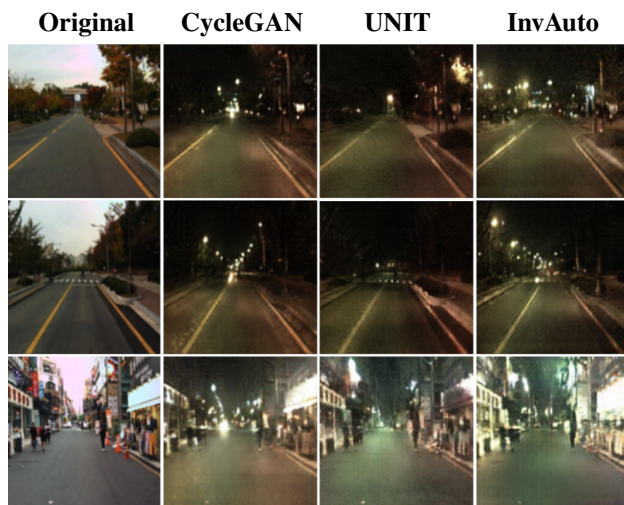


Figure 6. Day-to-night image conversion. Zoomed image is shown in Figure 18 in Section B of the Supplement.

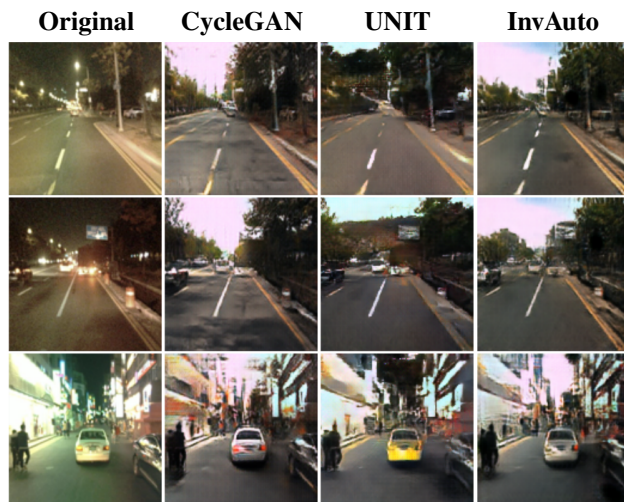


Figure 7. Night-to-day image conversion. Zoomed image is shown in Figure 19 in Section B of the Supplement.

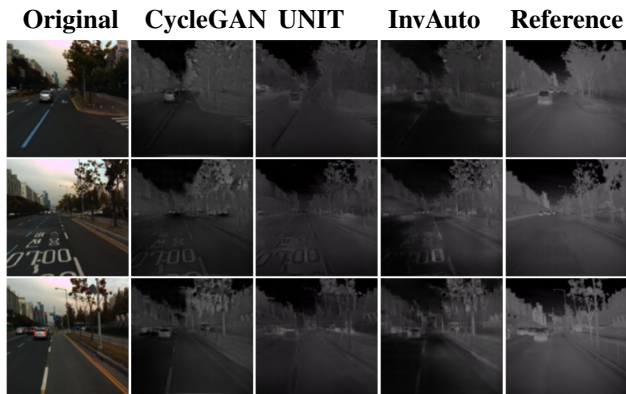


Figure 8. Day-to-thermal image conversion. Zoomed image is shown in Figure 20 in Section B of the Supplement.

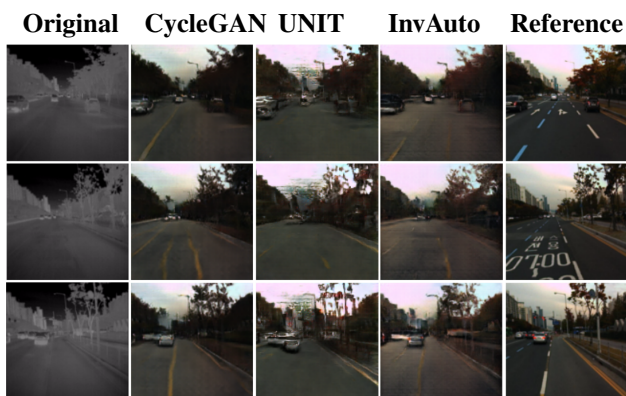


Figure 9. Thermal-to-day image conversion. Zoomed image is shown in Figure 21 in Section B of the Supplement.

To evaluate the performance of the methods numerically we use the following approach:

- For the tasks (ii) and (iii), we directly calculated the ℓ_1 loss between the converted images and the ground truth.
- For the task (i), we trained two autoencoders Ω_A and Ω_B on both domains, i.e. we trained each of them to reconstruct well the images from its own domain and reconstruct badly the images from the other domain. Then we use these two autoencoders to evaluate the quality of the converted images, where high ℓ_1 reconstruction loss of the autoencoder for the images converted to resemble those from its corresponding domain implies low-quality image translation.

Table 3 contains the results of the numerical evaluation and shows that the performance of InvAuto is similar to the state-of-the-art techniques that we compare InvAuto with and is furthermore contained within the performance range established by the CycleGAN (best performer) and UNIT (consistently slightly worst from CycleGAN).

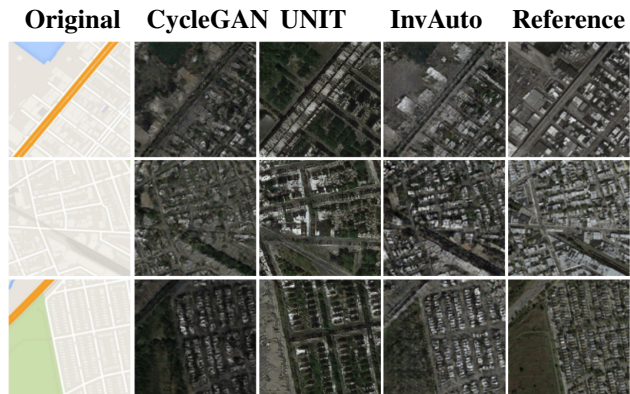


Figure 10. Maps-to-satellite image conversion. Zoomed image is shown in Figure 22 in Section B of the Supplement.

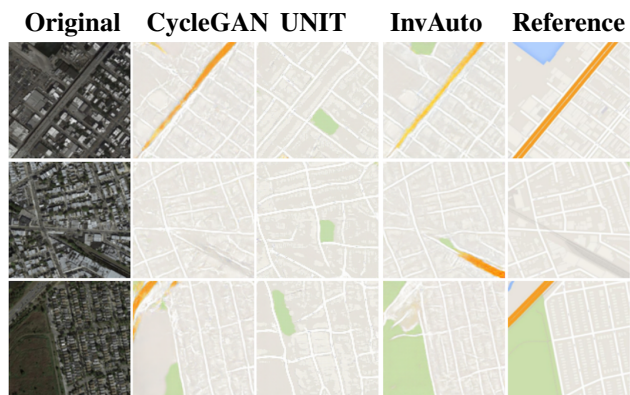


Figure 11. Satellite-to-maps image conversion. Zoomed image is shown in Figure 23 in Section B of the Supplement.

Tasks	Methods		
	CycleGAN	UNIT	InvAuto
Night-to-day	0.033	0.227	0.062
Day-to-nighth	0.041	0.114	0.067
Thermal-to-day	0.287	0.339	0.299
Day-to-thermal	0.179	0.194	0.205
Maps-to-satellite	0.261	0.331	0.272
Satellite-to-maps	0.069	0.104	0.080

Table 3. Numerical evaluation of CycleGAN, UNIT, and InvAuto.

5.2. Experiments with autonomous driving system

To test the quality of the image-to-image translations obtained by InvAuto, we use the NVIDIA evaluation system for autonomous driving described in details in (Bojarski et al., 2016). The system evaluates the performance of an already trained NVIDIA neural-network-based end-to-end learning platform for autonomous driving (PilotNet) on a test video using a simulator for autonomous driving. The system uses the following performance metrics for evaluation: autonomy, position precision, and comfort. We do not describe these metrics as they are described well in the mentioned paper. We only emphasize that these metrics are

expressed as a percentage, where 100% corresponds to the best performance. We collected the high-resolution videos of the same road during the day and night from the camera inside the car. Each video had $\sim 45\text{K}$ frames. The pictures were resized to 512×512 resolution for the conversion and then resized back to the original size of 1920×1208 . We used our domain translator as well as CycleGAN to convert the collected day video to a night video (Figure 12) and also the collected night video to a day video (Figure 13). To evaluate our model, we used aforementioned NVIDIA evaluation system, where the converted videos were used as testing sets for this system. We report results in Table 4.

Video type	Autonomy	Position precision	Comfort
Original day	99.6%	73.3%	89.7%
Original night	98.6%	63.1%	86.3%
Day-to-night InvAuto	99.0%	69.6%	83.2%
Night-to-day InvAuto	99.3%	68.0%	84.7%
Day-to-night CycleGAN	99.0%	68.4%	84.7%
Night-to-day CycleGAN	98.8%	64.0%	87.3%

Table 4. Experimental results with autonomous driving system: autonomy, position precision, and comfort.

The PilotNet model used for testing was trained mostly on day videos, thus it is expected to perform worse on night videos. Therefore the performance for original night video is worse than for the same video converted to a day video in terms of autonomy and position precision. The comfort deteriorates due to the inconsistency of consecutive frames in the converted video, i.e. the videos are converted frame-by-frame and we do not apply any post-processing to ensure smooth transition between frames. The results for InvAuto and CycleGAN are comparable.

6. Conclusion

We proposed a novel architecture that we call invertible autoencoder, which, as opposed to the common deep learning architectures, allows the layers of the model performing opposite operations (like encoder and decoder) to share weights. This is achieved by enforcing orthonormal mappings in the layers of the model. We demonstrate the applicability of the proposed architecture to the problem of domain adaptation and evaluate it on benchmark data sets and autonomous driving task. The performance of the proposed approach matches state-of-the-art methods and requires less trainable parameters.



Figure 12. Experimental results with autonomous driving system: day-to-night conversion. Zoomed image is shown in Figure 24 in Section B of the Supplement.

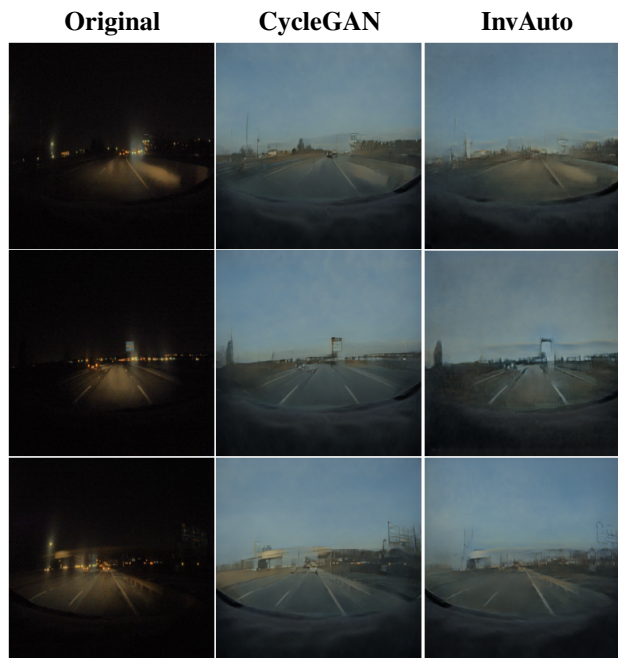


Figure 13. Experimental results with autonomous driving system: night-to-day conversion. Zoomed image is shown in Figure 25 in Section B of the Supplement.

References

Bojarski, M., Del Testa, D., Dworakowski, D., Firner, B., Flepp, B., Goyal, P., Jackel, L. D., Monfort, M.,

- Muller, U., Zhang, J., Zhang, X., Zhao, J., and Zieba, K. End to end learning for self-driving cars. *CoRR*, abs/1604.07316, 2016.
- Dong, H., Neekhara, P., Wu, C., and Guo, Y. Unsupervised image-to-image translation with generative adversarial networks. *CoRR*, abs/1701.02676, 2017.
- Gatys, L. A., Bethge, M., Hertzmann, A., and Shechtman, E. Preserving color in neural artistic style transfer. *CoRR*, abs/1606.05897, 2016a.
- Gatys, L. A., Ecker, A. S., and Bethge, M. Image style transfer using convolutional neural networks. In *CVPR*, 2016b.
- Goodfellow, I. J., Pouget-Abadie, J., Mirza, M., Xu, B., Warde-Farley, D., Ozair, S., Courville, A. C., and Bengio, Y. Generative adversarial nets. In *NIPS*, 2014.
- He, K., Zhang, X., Ren, S., and Sun, J. Deep residual learning for image recognition. In *CVPR*, 2016.
- Hwang, S., Park, J., Kim, N., Choi, Y., and Kweon, I. S. Multispectral pedestrian detection: Benchmark dataset and baseline. In *CVPR*, 2015.
- Isola, P., Zhu, J.-Y., Zhou, T., and Efros, A. A. Image-to-image translation with conditional adversarial networks. In *CVPR*, 2017.
- Johnson, J., Alahi, A., and Fei-Fei, Li. Perceptual losses for real-time style transfer and super-resolution. In *ECCV*, 2016.
- Kingma, D. P. and Ba, J. Adam: A method for stochastic optimization. *CoRR*, abs/1412.6980, 2014.
- Kingma, D. P. and Welling, M. Auto-encoding variational bayes. In *ICLR*, 2014.
- Liu, M.-Y. and Tuzel, O. Coupled generative adversarial networks. In *NIPS*. 2016.
- Liu, M.-Y., Breuel, T., and Kautz, J. Unsupervised image-to-image translation networks. In *NIPS*, 2017.
- McCann, M. T., Jin, K. H., and Unser, M. Convolutional neural networks for inverse problems in imaging: A review. *IEEE Signal Process. Mag.*, 34(6):85–95, 2017.
- Taigman, Y., Polyak, A., and Wolf, L. Unsupervised cross-domain image generation. *CoRR*, abs/1611.02200, 2016.
- Ulyanov, D., Lebedev, V., Vedaldi, A., and Lempitsky, V. S. Texture networks: Feed-forward synthesis of textures and stylized images. In *ICML*, 2016.
- Vasudevan, A., Anderson, A., and Gregg, D. Parallel multi channel convolution using general matrix multiplication. In *ASAP*, 2017.
- Vincent, P., Larochelle, H., Bengio, Y., and Manzagol, P.-A. Extracting and composing robust features with denoising autoencoders. In *ICML*, 2008.
- Wang, T.-C., Liu, M.-Y., Zhu, J.-Y., Tao, A., Kautz, J., and Catanzaro, B. High-resolution image synthesis and semantic manipulation with conditional gans. *CoRR*, abs/1711.11585, 2017.
- Zhu, J.-Y., Park, T., Isola, P., and Efros, A. A. Unpaired image-to-image translation using cycle-consistent adversarial networks. In *ICCV*, 2017.

Invertible Autoencoder for domain adaptation (Supplementary material)

A. Additional plots and tables for Section 3.6

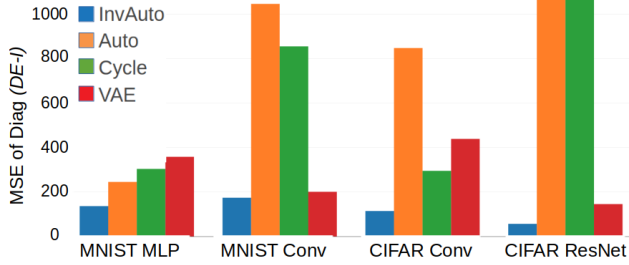


Figure 14. Comparison of the MSE of the diagonal of $DE - I$ for InvAuto, Auto, Cycle, and VAE on MLP, convolutional (Conv), and ResNet architectures and MNIST and CIFAR data sets.

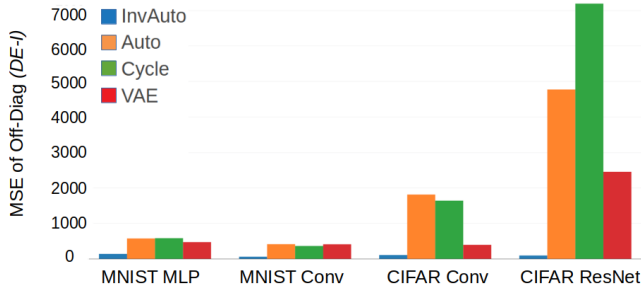


Figure 15. Comparison of the MSE of the off-diagonal of $DE - I$ for InvAuto, Auto, Cycle, and VAE on MLP, convolutional (Conv), and ResNet architectures and MNIST and CIFAR data set.

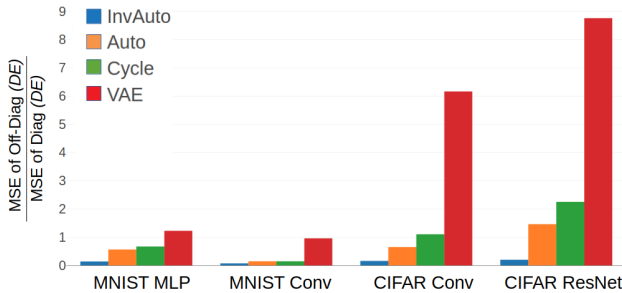


Figure 16. Comparison of the ratio of MSE of the off-diagonal and diagonal of DE for InvAuto, Auto, Cycle, and VAE on MLP, convolutional (Conv), and ResNet architectures and MNIST and CIFAR data sets.

Data set and model	InvAuto	Auto	Cycle	VAE
MNIST MLP	0.189	0.100	0.112	1.245
MNIST Conv	0.168	0.051	0.057	1.412
CIFAR Conv	0.236	0.126	0.195	1.457
CIFAR ResNet	0.032	0.127	0.217	0.964

Table 5. Test reconstruction loss (MSE) for InvAuto, Auto, Cycle, and VAE on MLP, convolutional (Conv), and ResNet architectures and MNIST and CIFAR data sets. VAE has significantly higher reconstruction loss by construction.

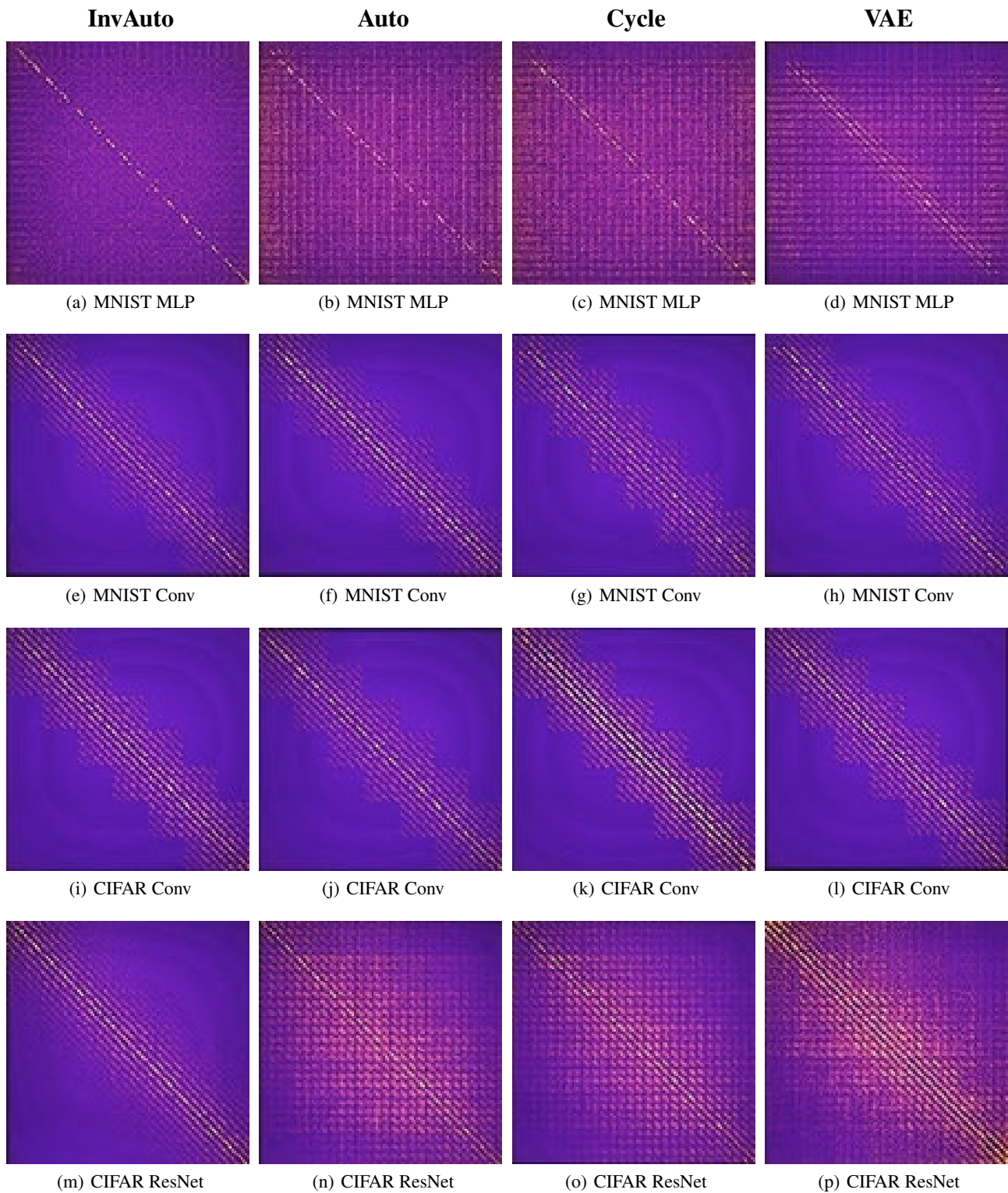


Figure 17. Heatmap of the values of matrix DE for InvAuto, (a,e,i,m) Auto (b,f,j,n), Cycle (c,g,k,o), and VAE (d,h,l,p) on MLP, convolutional (Conv), and ResNet architectures and MNIST and CIFAR data sets. Matrices E and D are constructed by multiplying the weight matrices of consecutive layers of encoder and decoder, respectively. In case of InvAuto, DE is the closest to the identity matrix.

B. Additional experimental results for Section 5

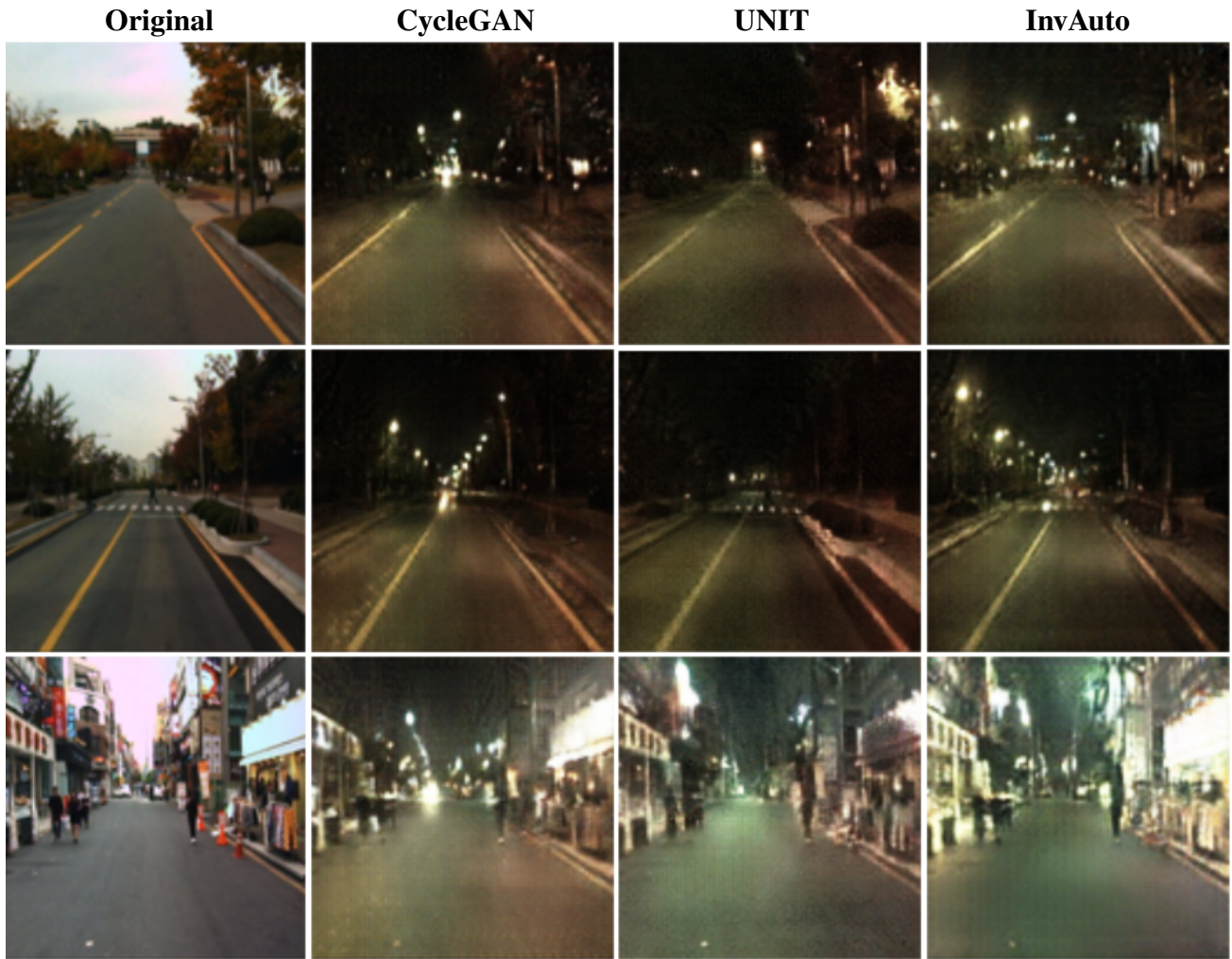


Figure 18. Day-to-night image conversion.



Figure 19. Night-to-day image conversion.

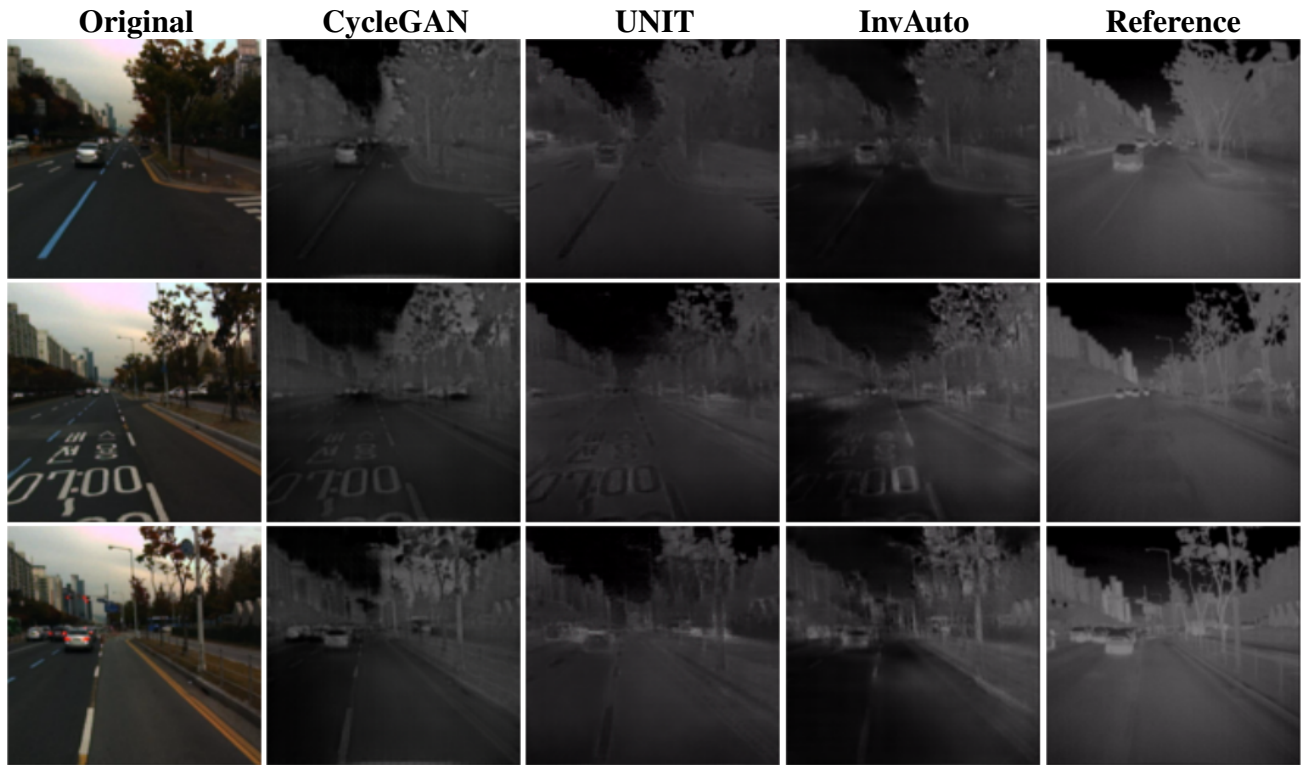


Figure 20. Day-to-thermal image conversion.

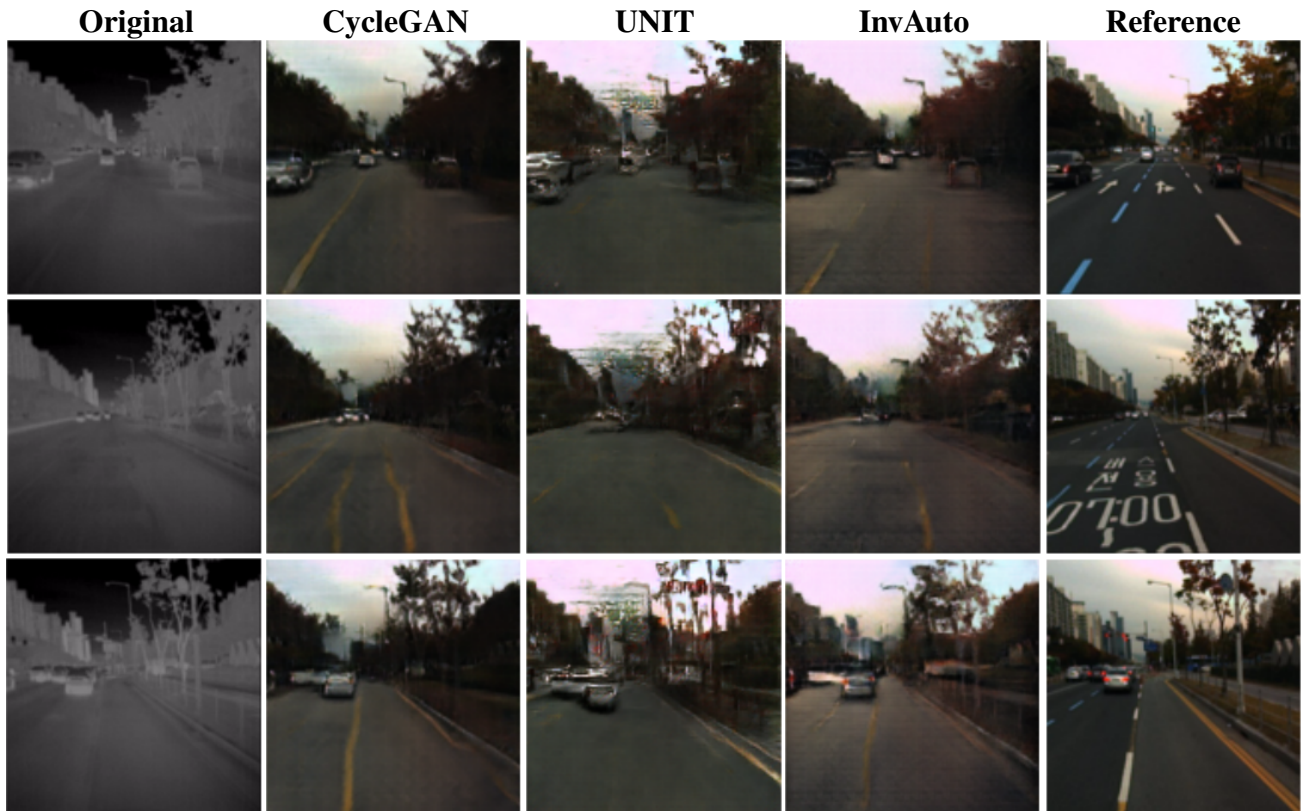


Figure 21. Thermal-to-day image conversion.

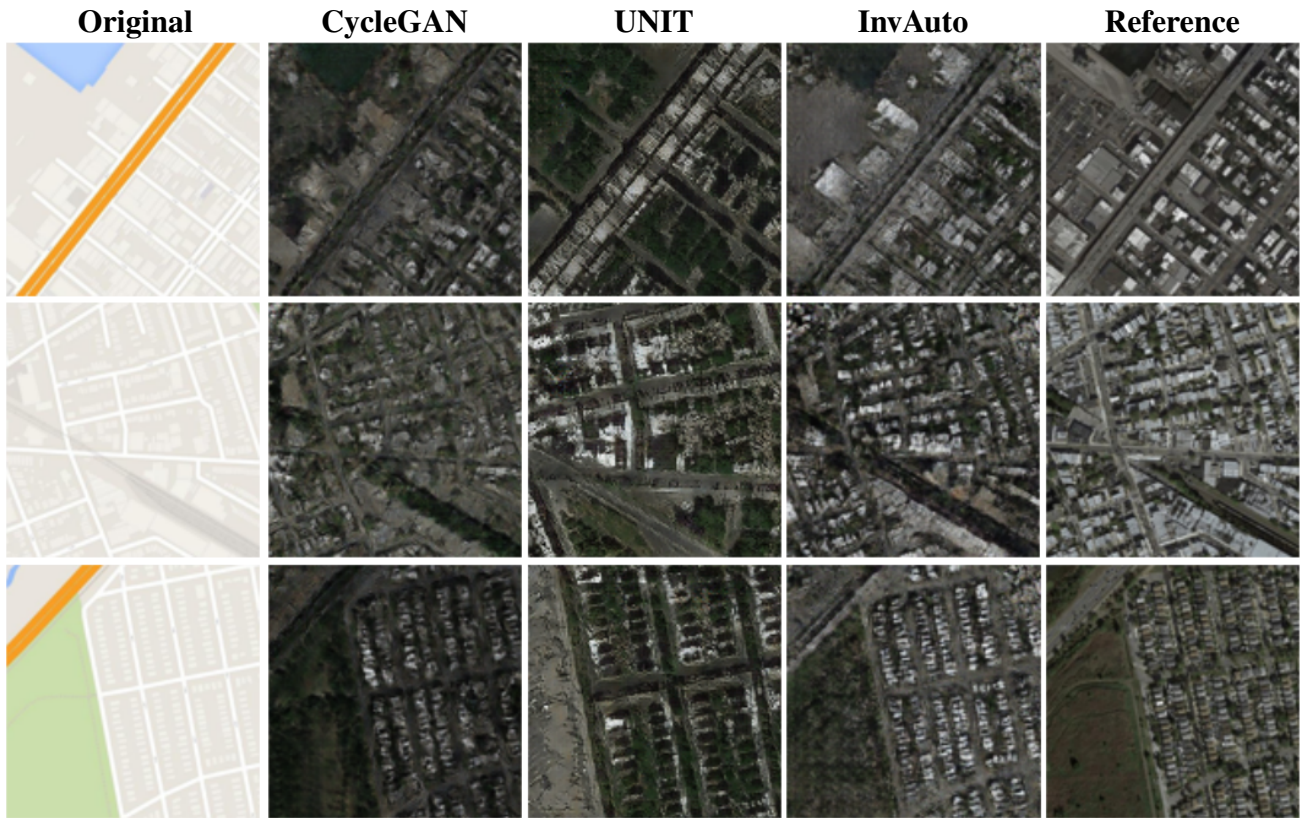


Figure 22. Maps-to-satellite image conversion.

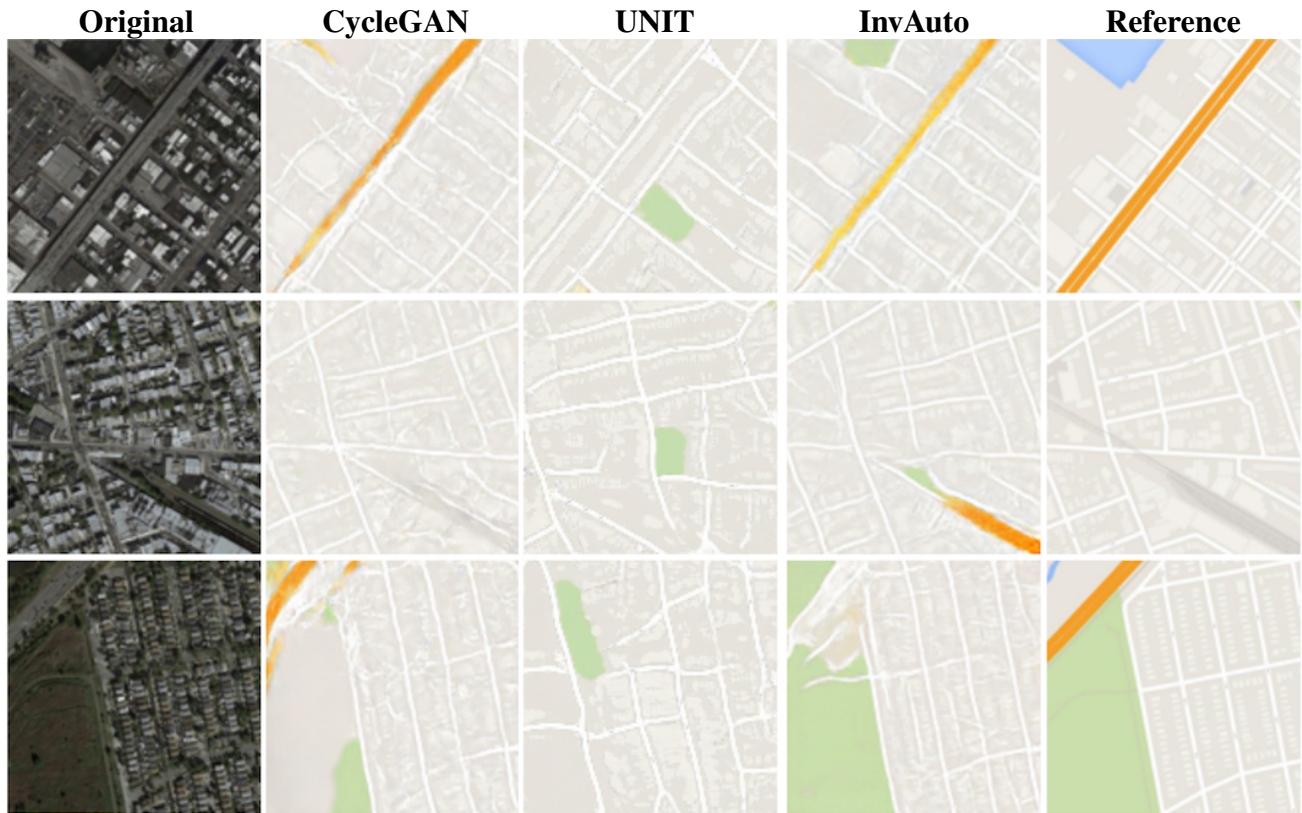


Figure 23. Satellite-to-maps image conversion.



Figure 24. Experimental results with autonomous driving system: day-to-night conversion.

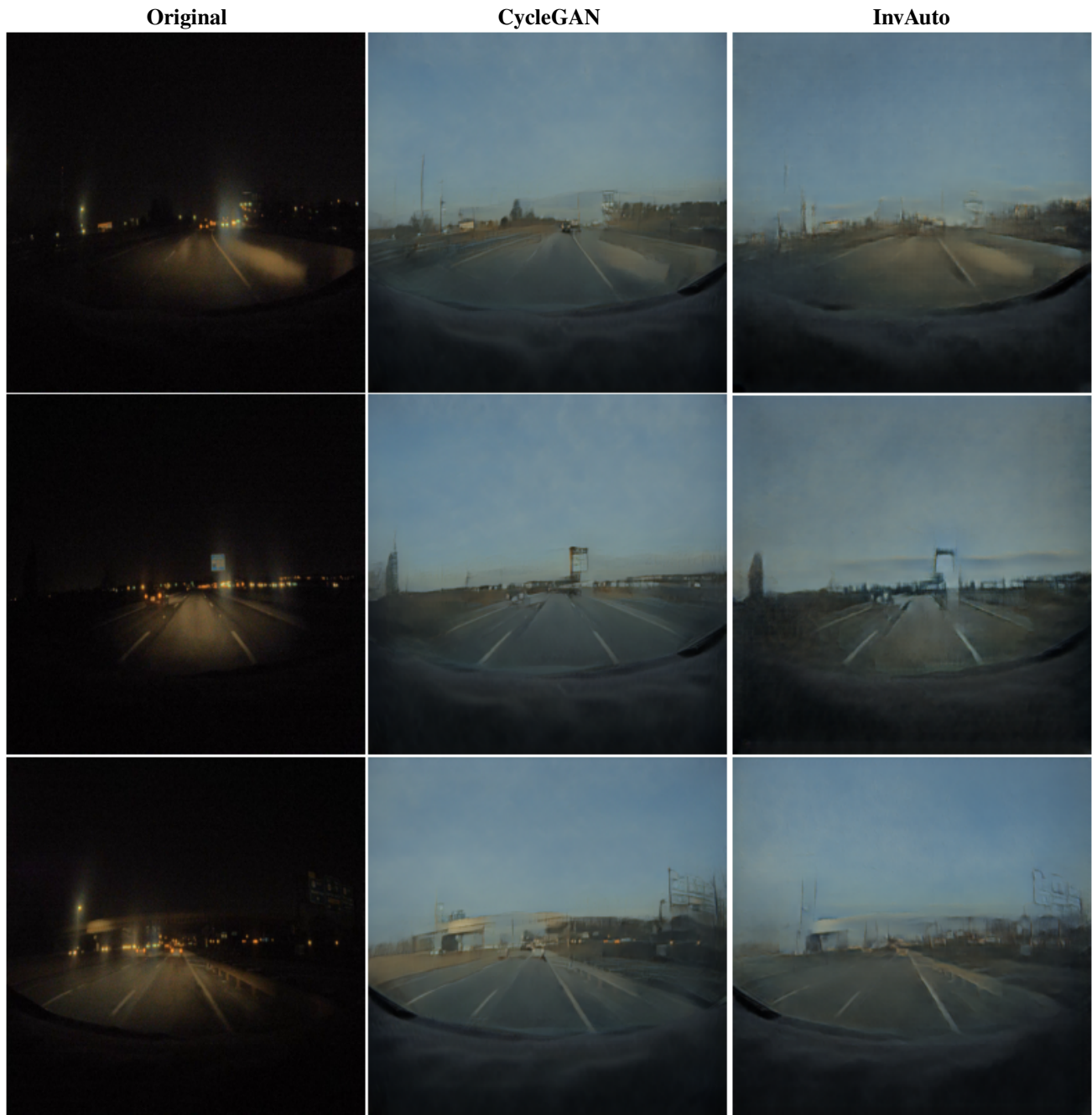


Figure 25. Experimental results with autonomous driving system: night-to-day conversion.

C. Invertible autoencoder for domain adaptation: architecture and training

Generator architecture Our implementation of InvAuto contains 18 invertible residual blocks for both 128×128 and 512×512 images, where 9 blocks are used in the encoder and the remaining in the decoder. All layers in the decoder are the inverted versions of encoder’s layers. We furthermore add two down-sampling layers and two up-sampling layers for the model trained on 128×128 images, and three down-sampling layers and three up-sampling layers for the model trained on 512×512 images. The details of the generator’s architecture are listed in Table 7 and Table 8. For convenience, we use Conv to denote convolutional layer, ConvNormReLU to denote Convolutional-InstanceNorm-LeakyReLU layer, InvRes to denote invertible residual block, and Tanh to denote hyperbolic tangent activation function. The negative slope of LeakyReLU function is set to 0.2. All filters are square and we have the following notations: K represents filter size and F represents the number of output feature maps. The paddings are added correspondingly.

Discriminator architecture We use similar discriminator architecture as PatchGAN (Isola et al., 2017). It is described in Table 6. We use this architecture for training both on 128×128 and 512×512 images.

Criterion and Optimization At training, we set $\lambda = 10$ and use l_1 loss for the cycle consistency in Equation 12. We use Adam optimizer (Kingma & Ba, 2014) with learning rate $l_r = 0.0002$, $\beta_1 = 0.5$ and $\beta_2 = 0.999$. We also add l_2 penalty with weight 10^{-6} .

Name	Stride	Filter
ConvNormReLU	2×2	K4-F64
ConvNormReLU	2×2	K4-F128
ConvNormReLU	2×2	K4-F256
ConvNormReLU	1×1	K4-F512
Conv	1×1	K4-F1

Table 6. Discriminator for both 128×128 and 512×512 images.

Name	Stride	Filter
ConvNormReLU	1×1	K7-F64
ConvNormReLU	2×2	K3-F128
ConvNormReLU	2×2	K3-F256
InvRes	1×1	K3-F256
InvRes	1×1	K3-F256
InvRes	1×1	K3-F256
InvRes	1×1	K3-F256
InvRes	1×1	K3-F256
InvRes	1×1	K3-F256
InvRes	1×1	K3-F256
InvRes	1×1	K3-F256
ConvNormReLU	$1/2 \times 1/2$	K3-F128
ConvNormReLU	$1/2 \times 1/2$	K3-F64
Conv	1×1	K7-F3
Tanh		

Table 7. Generator for 128×128 images.

Name	Stride	Filter
ConvNormReLU	1×1	K7-F64
ConvNormReLU	2×2	K3-F128
ConvNormReLU	2×2	K3-F256
ConvNormReLU	2×2	K3-F512
InvRes	1×1	K3-F512
InvRes	1×1	K3-F512
InvRes	1×1	K3-F512
InvRes	1×1	K3-F512
InvRes	1×1	K3-F512
InvRes	1×1	K3-F512
InvRes	1×1	K3-F512
InvRes	1×1	K3-F512
InvRes	1×1	K3-F512
ConvNormReLU	$1/2 \times 1/2$	K3-F256
ConvNormReLU	$1/2 \times 1/2$	K3-F128
ConvNormReLU	$1/2 \times 1/2$	K3-F64
Conv	1×1	K7-F3
Tanh		

Table 8. Generator for 512×512 images.